USP7 Inhibition Promotes Age-related Osteoporosis and Osteoporotic Osseointegration via Efferocytosis and Senolysis

Authors: Feng Zhou[1,2], Zhanqi Wang[1,2], Haiyun Li[1,2], Dongyang Wang[1,2], Zhongyu Wu[1,2], Fuwei Bai[1,2], Qingyi Wang[1], Wenxin Luo[1], Guorui Zhang[1], Yi Xiong[1,2], Yingying Wu[1,2]*

Affiliations:

[1]State Key Laboratory of Oral Diseases, National Clinical Research Center for Oral Diseases, West China Hospital of Stomatology, Sichuan University; Wuhou district, Chengdu, China

[2]Department of Oral Implantology, West China Hospital of Stomatology, Sichuan University; Wuhou district, Chengdu, China

*Corresponding author. Email: yywdentist@163.com.

Data and materials availability: All data are available in the main text or the supplementary materials.

Funding: National Natural Science Foundation of China (81970966, 82001084); Natural Science Foundation of Sichuan Province (2023NSFSC1513, 2023NSFSC0574)

Data and materials availability: All data are available in the main text or the supplementary materials.

Ethics approval statement: All animal experiments were approved by Subcommittee on Research and Animal Care (SRAC) of Sichuan University.

Word count: 9017

Main text word count: 5998

Reference count: 38

Figure count: 8

Abstract word count: 252

ABSTRACT

In elderly individuals, bone aging can lead to dysregulation of the bone immune microenvironment, resulting in the formation of osteoporotic microenvironment. Consequently, this can cause delayed bone fracture healing and early implant failure. Regarding osteoporotic microenvironment, the interaction between bone mesenchymal stem cells (BMSCs) and macrophages has gained increasing attention. Aged BMSCs exhibit a senescence-associated secretory phenotype (SASP). And SASP, together with macrophage inflammaging, contributes to the inflammatory microenvironment leading to osteoporosis and delayed bone healing. USP7, as a key deubiquitinase regulating cellular senescence and inflammation, has been found to promote senolysis when inhibited. This study investigated the effects of USP7 inhibition on aged BMSCs and bone marrow derived macrophages (BMDMs), as well as their interactive patterns. Through mRNA-Seq analysis, it was found that USP7 inhibition induced senolysis and osteogenic differentiation in aged BMSCs. For senescent BMDMs, USP7 inhibition suppressed NLRP3 inflammasome pathway and enhanced efferocytosis capacity through EPSIN1/LRP1 pathway, enabling them to efficiently clear apoptotic aged BMSCs caused by USP7 inhibition. Furthermore, by administering P5091 systemically to aged mice, it was discovered that USP7 inhibition could rescue bone loss and promote osseointegration of aged C57BL/6J mice via BMDMs efferocytosis and BMSCs senolysis. This study highlights the potential of USP7 inhibition in promoting senolysis in aged BMSCs and enhancing the efferocytosis capacity of senescent BMDMs, which exerts a synergistic therapeutic effect by inducing senescent cell

apoptosis and immune clearance. The "kill and bury" model proposed in this study for aged BMSCs-BMDMs crosstalk holds promise for future mechanistic research and drug development.

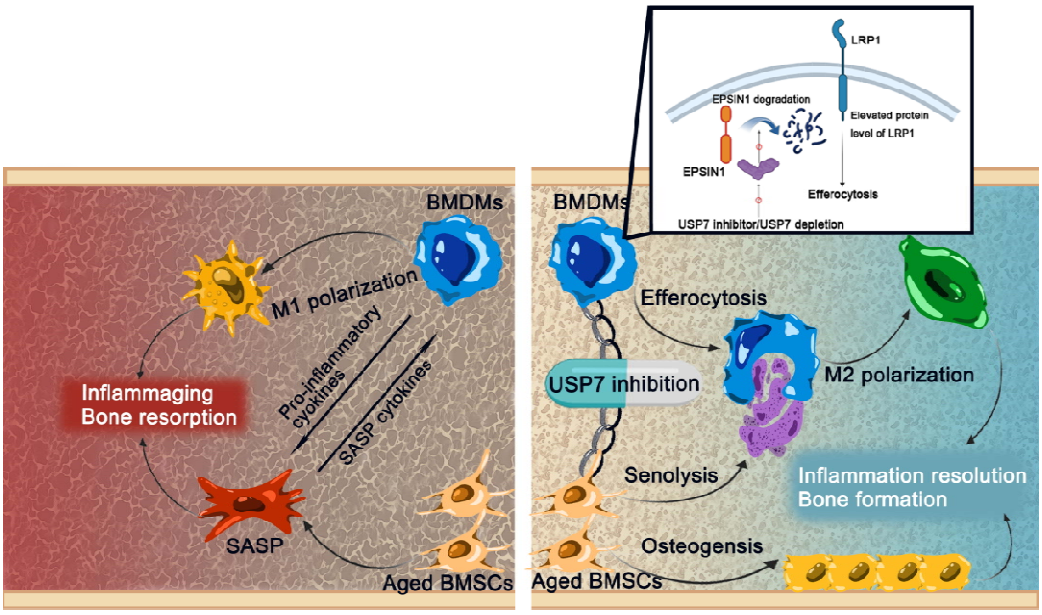

Lay summary:

The inflammatory osteoimmunology state is an important mechanism underlying age-related osteoporosis and delayed osseointegration. The interaction between BMSCs and macrophages may represent crucial therapeutic targets. On one hand, this study reveals that USP7 depletion could induce apoptosis of aged BMSCs through senolysis, while on the other hand, USP7 depletion could promote macrophage efferocytosis via the EPSIN1/LRP1 pathway, thereby clearing apoptotic aged BMSCs. This process simultaneously contributed to the clearance of senescent cells and the promotion of M2 polarization in macrophages. Moreover, *in vivo* experiments also demonstrate that USP7 inhibition improved age-related osteoporosis and osteoporotic

osseointegration by promoting senolysis and efferocytosis in aged mice, highlighting USP7 as a potential therapeutic target for bone aging-related diseases.

Key words: USP7, osteoporosis, osseointegration, osteoimmunology.

INTRODUCTION

Elderly people typically experience a decrease in bone mineral density and an increased risk of fractures, which is defined as osteoporosis (1). Moreover, elderly individuals frequently suffer from tooth loss. Nevertheless, as a critical treatment modality for tooth loss, dental implantation relies on the osseointegration, which is impeded by the osteoporotic microenvironment (2, 3). Conventional medications used for osteoporosis treatment, such as bisphosphonates, have detrimental impacts on the osseointegration of dental implants (4). Therefore, in recent years, drugs like vitamin D, which possess both osteogenesis-regulating and immunomodulatory functions, have gained widespread attention in research on osteoporosis and implant osseointegration (5). Consequently, exploring novel molecular mechanisms of osteoimmunology and drug targets may offer a dual benefit of improving both osteoporosis and osseointegration in elderly individuals.

In recent years, there has been increasing attention on the interaction between bone cells and immune cells in osteoporotic microenvironment. In this situation, the innate immune system plays a major role through pathways involving pathogen-associated molecular patterns (PAMPs), damage-associated molecular patterns (DAMPs), and

cellular stress (6). Numerous studies have revealed that overactive innate immune system in aged individuals can generate a chronic inflammatory microenvironment, which is called inflammaging (7). Inflammaging promotes osteoclast differentiation, inhibits osteoblast function, and consequently leads to bone loss and osteoporosis (8). Within the osteoporotic microenvironment, excessive activation of inflammation and osteoclast differentiation result in prolonged inflammation during the early stage of osseointegration, hindering macrophage polarization towards M2 phenotype and impeding osteogenic differentiation of stem cells (9). Therefore, the functional changes and interaction patterns between macrophages and bone mesenchymal stem cells (BMSCs) in the osteoporotic microenvironment can have a significant impact on the progression and treatment of osteoporosis and osteoporotic osseointegration.

Following this line of thought, the ubiquitin-proteasome system (UPS) is poised to become a key target for improving the aged BMSCs-macrophages crosstalk. UPS is the primary protein degradation system within eukaryotic cells, serving various functions such as clearing misfolded proteins, regulating cellular stress and signaling pathways, and controlling DNA damage repair (10). While this process is intricately regulated by the deubiquitination system. Peptidases, termed deubiquitinating enzymes (DUBs), can cleave the ubiquitin chains from substrate proteins, thereby sparing them from degradation (11). Among many family members of DUBs, USP7 has been recently discovered to have a role in regulating the aging process. He et al. found that inhibiting USP7 could selectively induce apoptosis in ionizing radiation-induced senescent fibroblasts, and the USP7 inhibitor P5091 could clear

senescent cells induced by doxorubicin in mice (12). This suggests that USP7 inhibition may be a potential approach for improving age-related diseases via senolysis. Senolysis and senotherapy refer to the selective removal of senescent cells without affecting normal cells, which can avoid tissue damage caused by senescent cells producing SASP cytokines like IL-1β and IL-6 (13). Therefore, we speculated that USP7 might be an important target for the treatment of age-related osteoporosis and osteoporotic osseointegration. The main objective of this study was to investigate the overall regulatory capability of USP7 on the interaction patterns between aged BMSCs and macrophages through *in vitro* mRNA-seq analysis. Furthermore, the impact of inhibiting USP7 *in vivo* on age-related bone homeostasis and osseointegration of dental implants was also examined. Thus, this study might help to explore the potential value of USP7 as a therapeutic target for bone aging-related diseases.

Materials and Methods

Study design

The objective of this study was to investigate the therapeutic effects of USP7 on age-related osteoporosis and osteoporotic osseointegration by focusing on the interaction between BMSCs and macrophages. Our goal was to propose a novel efferocytosis-senolysis combination therapy, offering new insights for future translational application. In *in vitro* experiments, BMSCs were obtained from young

and aged mice, and normal and senescent BMDMs were generated using conditional media of young and aged BMSCs. Subsequently, USP7 was depleted or inhibited using USP7 shRNA or USP7 inhibitor P5091. mRNA-Seq was then employed to explore the regulatory mechanisms of USP7 depletion in BMSCs and BMDMs. *In vivo* experiments were conducted by administering P5091 through intraperitoneal injection in both young and aged mice, simulating drug application as it would be in a clinical setting. We investigated the therapeutic effects of USP7 inhibition on bone loss in the femur and vertebrae, and on the osseointegration in maxillary dental implant. All mice were randomly assigned to different experimental groups. The sample size was determined based on previous publications and One-Way Analysis of Variance F-Test to obtain adequate statistical power. Investigations of all murine samples were performed in a blinded manner. All animal experiments were approved by Subcommittee on Research and Animal Care (SRAC) of Sichuan University. All data were biological replicates obtained from 3-6 independent experiments. No data were excluded in this study.

In vitro experiment

Cell culture and co-culture of BMSCs-BMDMs

BMSCs were cultured in the growth medium consisting of DMEM (Gibco), supplemented with 10% FBS (Gibco), and 1% penicillin and streptomycin. BMDMs were plated in pre-cooled prepared bone marrow macrophage differentiation medium containing DMEM (Gibco), 10% FBS (Gibco), 1% penicillin/streptomycin, and 20 ng/mL monocyte-colony stimulating factor (M-CSF, PeproTech). In the indirect

co-culture system, 0.4 μm 24-well Transwell inserts were utilized to co-culture BMSCs and BMDMs. As for the direct co-culture system, a 24-well plate was used to co-culture BMSCs and BMDMs. A total of 60,000 BMSCs and 60,000 BMDMs were simultaneously seeded into the 24-well plate, and 500 μL of growth medium containing 20 ng/mL M-CSF was added.

mRNA-seq

The transcriptome sequencing and subsequent analysis were conducted by OE Biotech Co., Ltd. (Shanghai, China). Briefly, total RNAs were extracted utilizing the TRizol reagent (Invitrogen). The purity and concentration of the RNA were determined with a NanoDrop 2000 spectrophotometer (Thermo Scientific). Subsequently, libraries were prepared in accordance with the manufacturer's protocol using the VAHTS Universal V6 RNA-seq Library Prep Kit. The libraries were subjected to sequencing on an Illumina Novaseq 6000 platform, yielding 150 bp paired-end reads. Quality control of the mRNA-seq data was carried out using FastQC (v0.11.5) and the FASTX toolkit (0.0.13). Alignment to the Mus musculus reference genomes was performed using HISAT2 (v.2.0.4). Differentially expressed genes between sh*Usp7* and shNC groups were identified using the DEseq2 package (version 1.34.0) if they met the criteria of Q value < 0.05 and a fold change greater than 2 or less than 0.5.

Lentivirus transfection, cell proliferation assay, migration assay and other in vivo experiments

See the Supplemental Materials and Methods for details.

In vivo experiment

Mice

All animal experiments were approved by Subcommittee on Research and Animal Care (SRAC) of Sichuan University. Young (3-month-old) and aged (20-month-old) male wild-type C57BL/6J mice were purchased from Chengdu Dossy Experimental Animals Co. Ltd. These mice were accommodated at the Experimental Animal Center of Sichuan University. The mice were fed a standard chow diet without restrictions and were kept in an environment with a 12-hour light and 12-hour dark cycle. Young or aged mice were randomly assigned to 5 per cage. The sample size was determined based on former studies. USP7 inhibitor P5091 was dissolved in PBS containing 4% DMSO. Mice were injected daily i.p. with injections of vehicle (4% DMSO in PBS) or P5091 (15 mg/kg) or receptor-associated-protein (RAP, 20mg/kg) for 28 days. For the mice used in double bone labeling assay, mice were injected with calcein (10 mg/kg) and alizarin red (20 mg/kg) at 10 days and 3 days prior to euthanasia. All animal experiments described above were conducted in accordance with the ARRIVE guidelines.

Implant surgery

All mice were were anesthetized via intraperitoneal injection of ketamine at 80 mg/kg (Sigma Chemical) and xylazine at 10 mg/kg (Sigma Chemical). Following oral saline cleaning, a 2 mm incision was made anterior to the left first upper molars to mark the

implant site. The implant site was prepared under saline cooling using a surgical motor (NSK-Nakanishi). Subsequently, the pilot hole was adjusted to accommodate the titanium implant (WEGO) using a drill. The titanium implant was then screwed into the implant bed with a screwdriver. Following the surgery, the mice were provided with a soft diet and were injected daily *i.p.* with injections of vehicle (4% DMSO in PBS) or P5091 (15 mg/kg) for 4 weeks.

MicroCT and histomorphometric/immunofluorescence staining analysis

See the Supplemental Materials and Methods for details.

Statistical analysis

Statistical analyses were conducted using GraphPad Prism version 8.0. The data are expressed as means with standard deviation (SD). Student's t-test was employed to compare two groups, while one-way analysis of variance (ANOVA) was applied when analyzing more than two groups. For multiple comparisons, the Bonferroni's multiple comparisons test was utilized. Sample sizes are specified in the figure legends. Statistical significance was defined as $P < 0.05$.

Results

USP7 inhibition ameliorates inflammaging of senescent macrophages

To assess the impact of USP7 depletion on senescent macrophages, the following experimental procedures were conducted. The conditioned media (CM) derived from young BMSCs and aged BMSCs was designated as control CM and senescent CM.

BMDMs cultured with control CM were employed as the control group (CON) to simulate normal BMDMs, whereas BMDMs cultured with senescent CM were represented as senescent group (SEN) (Fig. 1A).

Subsequently, shRNA targeting *Usp7* was transfected into BMDMs to deplete USP7 expression (Fig. S1A-B). mRNA-Seq analysis was performed on senescent BMDMs, revealing a notable downregulation of genes associated with the innate immune response pathway and NLRP3 pathway in USP7-depleted BMDMs (Fig. 1B). Gene set enrichment analysis (GSEA) demonstrated a decreased activity of the innate immune response and NLRP3 pathway in USP7-depleted senescent BMDMs (Fig. 1C-D). Results obtained from qPCR validated the results of GSEA, demonstrating significantly upregulated inflammation mRNA expression in senescent BMDMs compared to normal BMDMs. And USP7 depletion suppressed the expression of these genes in senescent BMDMs (Fig. 1E). Furthermore, Western blot indicated that NLRP3 pathway was downregulated by USP7 depletion in senescent BMDMs (Fig. 1F-G). Additionally, the secretion of IL-1β and IL-6 in the culture media of senescent BMDMs was reduced following USP7 depletion (Fig. 1H). As for macrophage polarization, results of flow cytometry indicated that M2/M1 ratio was significantly increased in senescent BMDMs upon USP7 depletion (Fig. 1I).

Moreover, a selective USP7 inhibitor, P5091, was employed to investigate the role of USP7 inhibition in BMDMs inflammaging. Based on CCK8 assays, the optimal concentration for treating BMDMs and BMSCs was determined to be 5μM (Fig. S1C). Although P5091 had minimal effects on normal BMDMs, it significantly inhibited

inflammation mRNA expression in senescent BMDMs (Fig. S1D). Additionally, P5091 suppressed the secretion of IL-1β and IL-6 in the culture media of senescent BMDMs (Fig. S1E). Western blot analysis further indicated that P5091 inhibited the NLRP3 pathway in senescent BMDMs without affecting the protein levels of NLRP3 and cleaved IL-1β in normal BMDMs (Fig S1F-H).

USP7 inhibition enhanced aged BMSCs osteogenesis co-cultured with macrophages

Subsequently, we investigated the influence of senescent BMDMs on BMSCs. A transwell co-culture model was employed to facilitate this investigation. Initially, the upper chamber was seeded with USP7-depleted or normal BMDMs, while the lower chamber contained young or aged BMSCs (Fig. 2A). While, as for transwell migration assay, BMSCs were placed in the upper chamber and BMDMs were placed in the lower chamber, to evaluate cell migration (Fig. 2B). CCK8 assay revealed that USP7-depleted BMDMs significantly enhanced the proliferation of young BMSCs, while exerting limited effects on aged BMSCs (Fig. 2C). In contrast to the results from the CCK8 assay, USP7-depleted BMDMs significantly inhibited the migration of young BMSCs. However, USP7-depleted BMDMs promoted the migration of aged BMSCs (Fig. 2D). Furthermore, the osteogenesis potential of BMSCs was examined using ALP and ARS staining. The aged BMSCs co-cultured with BMDMs exhibited inhibited osteogenesis. In contrast, USP7-depleted BMDMs rescued the impaired osteogenesis (Fig. 2E). Consistent with this, qPCR analysis demonstrated that aged BMSCs co-cultured with BMDMs exhibited lower osteogenesis mRNA expression.

However, USP7 depletion enhanced the expression of these genes (Fig. 2H). Additionally, Western blot revealed decreased osteogenesis protein levels in aged BMSCs co-cultured with BMDMs, while USP7-depleted BMDMs significantly upregulated their expression (Fig. 2G-H). Moreover, SA-β-gal staining demonstrated significant senescence phenotype in aged BMSCs, however, USP7-depleted BMDMs reduced the senescence status in aged BMSCs (Fig. 2I). Moreover, the expression of SASP markers, such as *Il-1b*, *Il-6*, and *p53*, were evaluated using qPCR (Fig. 2J). The results indicated that USP7-depleted BMDMs could reduce SASP markers of aged BMSCs.

Next, we conducted further investigations to examine the effects of P5091 in the BMDMs-BMSCs interaction system (Fig.S2A-B). P5091 significantly inhibited BMSCs proliferation in the aged BMDMs-BMSCs system (Fig.S2C). However, P5091 promoted aged BMSCs migration when co-cultured with BMDMs (Fig.S2D). As for osteogenesis potential, ALP and ARS staining showed that P5091 also promoted osteogenesis capacity of aged BMSCs with BMDMs (Fig. S2E). The mRNA expression of *Alp* and *Col1a1* were upregulated in aged BMSCs with BMDMs under P5091 treatment (Fig. S2F). We further evaluated the protein levels of osteogenesis markers and found that P5091 significantly promoted the expression of ALP, RUNX2, and COL1A1 in aged BMSCs co-cultured with BMDMs. In contrast, expression of COL1A1 in young BMSCs were inhibited after P5091 application (Fig. S2G-H). Additionally, SA-β-gal staining and SASP mRNA expression were also reduced in aged BMSCs under P5091 treatment (Fig. S2I-J).

USP7 inhibition promotes osteogenesis of senescent BMSCs via senolysis

Next, we attempted to investigate the effects of USP7 depletion and P5091-mediated USP7 inhibition on BMSCs. Initially, we successfully knocked down USP7 expression in BMSCs (Fig. S3A-B). Firstly, through mRNA-Seq analysis, GSEA showed that USP7 depletion in aged BMSCs lead to a reduction in the SASP, promotion of osteogenic differentiation, and induction of cell apoptosis (Fig. 3A-B). Furthermore, CCK8 assays revealed that USP7 depletion enhanced cell proliferation of young BMSCs but attenuated the proliferation of aged BMSCs (Fig. 3C). Transwell migration assays also confirmed that USP7 depletion promoted the migration of aged BMSCs (Fig. 3D).

Regarding osteogenic capacity, ALP and ARS staining showed that USP7 depletion weakened the osteogenic potential of young BMSCs, while significantly enhanced the osteogenic capacity of aged BMSCs (Fig. 3E). qPCR analysis revealed an increase in the osteogenesis mRNA expression levels upon USP7 depletion in aged BMSCs (Fig. 3F). Western blot analysis also indicated that USP7 depletion caused a significant reduction in the protein levels of ALP and COL1A1 in young BMSCs, while rescuing these markers in aged BMSCs (Fig. 3G-H).

Subsequently, we explored whether USP7 exhibited senolytic effects. USP7 depletion significantly reduced the number of SA-β-gal-positive cells and the SASP phenotype in aged BMSCs (Fig. 3I-J). Live-dead cell staining also revealed that USP7 depletion promoted cell death specifically in aged BMSCs without affecting young BMSCs (Fig. 3K, M). Flow cytometry results indicated that USP7 depletion had minimal impact on

apoptosis levels in young BMSCs, whereas it significantly increased the proportion of apoptotic cells in aged BMSCs (Fig. 3L, N)

In addition to using shRNA, we also employed P5091 to inhibit USP7 in BMSCs. Firstly, P5091 significantly inhibited the proliferation of both young and aged BMSCs (Fig. S3C). However, P5091 significantly enhanced the migration activity of aged BMSCs (Fig. S3D). In terms of osteogenic capacity, ALP staining indicated that P5091 significantly increased the early osteogenic potential of aged BMSCs. However, ARS staining revealed that P5091 diminished the mineralization ability of young BMSCs while significantly enhanced the mineralization ability of aged BMSCs (Fig. S3E). Moreover, qPCR experiments demonstrated that P5091 markedly increased the expression of *Alp* in aged BMSCs (Fig. S3F). Regarding the protein level, we observed that P5091 significantly suppressed the expression of osteogenesis proteins in young BMSCs, while substantially increasing the expression of these proteins in aged BMSCs (Fig. S3G-H). Furthermore, we investigated the effects of P5091 as a potential senolytic drug. P5091 reduced the number of SA-β-gal-positive cells and suppressed the expression of SASP-related genes (Fig. S3I-J). Similar to the effect of shRNA, live-dead cell staining and flow cytometry results indicated that P5091 increased apoptosis levels in aged BMSCs without affecting young BMSCs (Fig. S3K-L).

USP7 inhibition rejuvenates efferocytosis in senescent macrophages partially through upregulating LRP1

In order to further investigate the interaction between macrophages and bone stem cells in the bone microenvironment, we utilized a recently published single-cell dataset (GSE169396) that encompasses samples from four human femoral heads (Fig. 4A). In this context, we observed that TAM (Tyro3, Axl, and MerTK) receptors, responsible for recognizing apoptotic cells, were primarily expressed in macrophages, while the TAM ligand Gas6 was predominantly expressed in the osteoblastic lineage (Fig. 4B-E). This suggests a potential crosstalk of efferocytosis between BMDMs and BMSCs in the bone marrow microenvironment. Therefore, upon further analysis of the mRNA-Seq results from senescent BMDMs with USP7 depletion, we observed a significant upregulation in the expression of efferocytosis-related genes in senescent USP7-depleted BMDMs (Fig.4F). Through GSEA, we found that the apoptotic cell clearance pathway was significantly enhanced in USP7-depleted senescent BMDMs (Fig. 4G-H). qPCR showed that key efferocytosis genes, *Cd36*, *Mertk*, and *Lrp1*, were significantly upregulated in USP7-depleted BMDMs (Fig. S4). Because researches have found that LRP1 plays a significant role in both bone homeostasis and macrophage efferocytosis, we focused on investigating the role of LRP1 (14). The use of LRP1 inhibitor receptor-associated-protein (RAP) significantly inhibited the expression of efferocytosis-related genes (Fig. S4). Subsequently, we labeled Jurkat cells with calcein-AM and co-cultured them with BMDMs to evaluate efferocytosis efficiency. The results revealed that the efferocytosis ability of senescent BMDMs was significantly reduced, but USP7 depletion significantly enhanced the efferocytosis capacity of senescent BMDMs. However, RAP counteracted the effect of USP7

depletion on efferocytosis (Fig. 4I-J). Furthermore, we quantitatively measured efferocytosis efficiency through flow cytometry. Using DiIC18(5)-DS to label apoptotic Jurkat cell membranes, we calculated the ratio of DiIC18(5)-DS and F4/80 double-positive cells to determine efferocytosis efficiency. The results demonstrated that USP7 depletion significantly increased the efferocytosis efficiency of senescent BMDMs, while RAP weakened the promoting effect of USP7 depletion (Fig. 4K-L).

Considering that efferocytosis plays a crucial role in promoting M2 polarization of macrophages, we investigated the effects of USP7 depletion on M2 polarization and osteogenic regulation in BMDMs after efferocytosis. Flow cytometry analysis of BMDMs co-cultured with apoptotic cells revealed that the proportion of CD206-positive M2 cells in senescent BMDMs was significantly reduced compared to the young group. However, USP7 depletion rescued this reduction. And RAP partially antagonized the promoting M2 polarization effect (Fig. S5A). Further, we directly co-cultured BMDMs with aged BMSCs and performed ALP and ARS staining. The results showed that sole USP7 depletion in BMDMs or BMSCs promoted osteogenesis compared to the NC groups of BMDMs or BMSCs, but the group with simultaneous USP7 depletion in both BMDMs and BMSCs exhibited the strongest osteogenic ability. However, LRP1 depletion in BMDMs weakened the pro-osteogenic capacity compared to that of BMDMs without *Lrp1* depletion (Fig. S5B). Finally, qPCR results revealed that USP7 depletion in BMDMs co-cultured with apoptotic cells significantly upregulated anti-inflammatory gene expression and downregulated pro-inflammatory gene expression. However, RAP partially counteracted this effect (Fig. S5C).

USP7 inhibition orchestrates EPSIN1/LRP1 pathway to enhance efferocytosis

Next, we delved deeper into the specific pathway through which USP7 promotes efferocytosis in senescent BMDMs. Firstly, we established macrophage models overexpressing HA-USP7 and Flag-EPSIN1. By using cycloheximide (CHX) to treat macrophages, we observed that under conditions of protein synthesis inhibition, EPSIN1 was gradually degraded. After USP7 depletion, the expression of EPSIN1 protein significantly decreased (Fig. 5A). Conversely, USP7 overexpression led to a marked increase in EPSIN1 expression (Fig. 5B). Subsequently, through co-IP, we further confirmed the protein interaction between USP7 and EPSIN1, as well as between HA-USP7 and Flag-EPSIN1 (Fig. 5C-D)).

Furthermore, we found that in senescent BMDMs, both USP7 and EPSIN1 expression increased, while LRP1 expression decreased. USP7 depletion reversed this trend (Fig. 5E). Additionally, the ubiquitination level of EPSIN1 in senescent BMDMs decreased, but USP7 depletion significantly increased EPSIN1 ubiquitination levels (Fig. 5F).

Next, we explored the interaction and ubiquitination status of the HA-USP7 and Flag-EPSIN1 system. The results revealed that the overexpression of these proteins did not affect the overall ubiquitin protein levels within BMDMs (Fig. 5G). However, in BMDMs overexpressing HA-USP7, the ubiquitination level of FLAG-EPSIN1 significantly decreased, indicating that HA-USP7 also possesses the ability to deubiquitinate Flag-EPSIN1 (Fig. 5H).

In summary, the results above suggested that there might be an abnormally high expression of USP7 in senescent BMDMs, leading to deubiquitination and reduced degradation of EPSIN1, subsequently resulting in excessive degradation of LRP1 and inhibition of efferocytosis. USP7 depletion increases EPSIN1 ubiquitination levels and degradation, thus allowing LRP1 to be protected from degradation and facilitating efferocytosis (Fig. 5I).

USP7 inhibition promotes osteoporosis via efferocytosis in aged mice

To validate the *in vivo* effects of USP7 inhibition, we investigated the impact of USP7 inhibition on age-related osteoporosis. Firstly, after P5091 injection, MicroCT revealed a significant increase in bone mass in the femurs of aged mice, while changes in trabecular bone structure were not significant. However, RAP reversed the osteogenesis-promoting effect of P5091 (Fig. 6A-B). In the thoracic vertebrae, we observed that P5091 significantly increased bone mass and trabecular number, but RAP attenuated the therapeutic effect of P5091 (Fig. S6A-B). Furthermore, H&E staining of femurs showed a significant increase in trabecular number after P5091 injection in aged mice (Fig. 6C). Bone double-labeling fluorescence staining also indicated a noticeable increase in mineralization deposition area and rate in aged mice after P5091 injection (Fig. 6D-E). Combined with the results of ALP immunohistochemical staining, we found that this might be related to an increase in osteoblast numbers in trabecular bone following P5091 injection (Fig. 6F-G). We further examined femur samples through qPCR, which showed elevated expression of *Alp*, *Runx2*, and *Col1a1* in aged femurs tissue after P5091 injection (Fig. 6H). We

also assessed the systemic effects of P5091 injection in mice. We found that P5091 significantly reduced the levels of IL-1β and IL-6 in the serum of aged mice (Fig. 6I). And simultaneously, P5091 decreased the area of lipid droplets in the liver of aged mice (Fig. S6C). However, unlike in bone tissue, RAP did not affect the efficacy of P5091 in other parts of the body.

Furthermore, we investigated whether P5091 could promote efferocytosis in bone tissue. We used TUNEL staining to label apoptotic cells and used F4/80 and DAPI to label macrophages to observe the phenomenon of macrophages engulfing apoptotic cells (Fig. 6J). We found that in the femurs of aged mice, the numbers of apoptotic cells and macrophages were significantly reduced. P5091 significantly increased the numbers of apoptotic cells and macrophages in aged mice, and RAP did not affect the number of apoptosis cells and macrophages (Fig. 6K). At the same time, the efferocytosis function in femoral tissue of aged mice was significantly weakened, and P5091 significantly increased the ratio of macrophages engulfing apoptotic cells. However, the application of RAP significantly attenuated the efferocytosis-promoting effect of P5091.

USP7 inhibition enhances osseointegration of dental implants in aged mice

In addition to osteoporosis, we further investigated the impact of USP7 inhibition on osseoporotic osseointegration in aged mice, we initially established a mouse maxillary edentulous ridge implantation model (Fig. 7A). MicroCT results revealed that the bone volume and osseointegration rate around the implants in aged mice were significantly lower than those in young mice at both early (2 weeks) and late (4 weeks)

stage of osseointegration. However, P5091 treatment primarily enhanced osseointegration in aged mice during the late stage of osseointegration (4w). Concurrently, the application of RAP attenuated the beneficial effect of P5091 on osseointegration (Fig. 7B). Similar to the MicroCT results, H&E staining indicated that at 2 weeks post-implantation, young mice exhibited evident bone tissue formation around the implants, whereas aged mice predominantly displayed fibrous connective tissue. By 4 weeks, aged mice treated with P5091 showed noticeable woven bone structure formation around the implants, while Veh group and Veh+RAP group showed no significant bone structure formation (Fig. S8A). Subsequently, we examined osteogenesis and osteoclastic activity around the implants. ALP staining revealed a higher number of osteoblasts and increased ALP expression in the peri-implant region of young mice. In aged mice at 2 weeks post-implantation, P5091 significantly increased the number of osteoblasts (Fig. 7C). Similarly, qPCR results revealed that bone tissue around implants expressed less osteogenic genes in aged mice compared to young mice, while P5091 upregulated both in 2w and 4w (Fig. S8B). Regarding osteoclastic activity, we utilized TRAP staining to observe the number and surface ratio of osteoclasts around the implants. The results indicated that at 2 weeks, there was no significant difference in the number and surface of osteoclasts between aged and young mice, and the effect of P5091 was also not significant. Interestingly, the use of RAP significantly downregulated both the number and surface of osteoclasts. At 4 weeks post-implantation, the number and surface of osteoclasts around the implants in young mice were significantly reduced, whereas

aged mice still maintained a relatively high level. And P5091 downregulated the number and surface of osteoclasts around the implants (Fig. 7D). This observation may suggest that the delayed osseointegration in aged mice is partially attributed to the prolonged excessive osteoclastic activity.

USP7 inhibition promoted efferocytosis during osseointegration in aged mice

Similar to observations in the femurs, we employed TUNEL and F4/80 immunofluorescence staining to assess changes in the number of apoptotic cells and the level of efferocytosis around the implants (Fig. 8A). At 2 weeks post-implantation, in young mice, P5091 did not significantly alter the number of apoptotic cells, macrophage counts, or efferocytosis levels. However, in aged mice, P5091 significantly increased the number of apoptotic cells and macrophages, and notably promoted efferocytosis. While the use of RAP did not alter the number of apoptotic cells, it significantly reduced the number of macrophages and suppressed efferocytosis (Fig. 8B-D). At 4 weeks post-implantation, both in young and aged mice, there were relatively fewer apoptotic cells and macrophages around the implants, and efferocytosis was also not evident (Fig. S9). This indicates that during the process of osseointegration, phenomena such as cell apoptosis, macrophage migration, and efferocytosis primarily occur in the early stage of osseointegration.

DISCUSSION

In recent years, various anti-aging drugs have been attempted for the treatment of bone aging, involving multiple mechanisms such as anti-inflammation, antioxidative stress, and promotion of osteogenesis (15). A study on C. elegans found that ubiquitination/deubiquitination imbalance might be an endogenous mechanism of organismal aging (16). In aging individuals, there is an increase in the expression of deubiquitinating enzymes, leading to a decrease in overall ubiquitination levels within cells. This results in the accumulation of abnormal proteins, causing cellular dysfunction and senescence. Therefore, inhibiting DUBs, such as USP7 inhibitor P5091, may represent a crucial target for anti-aging therapies. However, research on the role of USP7 and P5091 in bone remodeling is still limited.

In this study, we initially investigated the effects of USP7 inhibition on the inflammaging of BMDMs. Ambrosi et al. found that aged skeletal stem cells in the bone marrow of aged mice possess the ability to create an inflammatory microenvironment, driving osteoclast differentiation and myeloid skewing (17). However, in *in vitro* experiments, Yin et al. co-cultured young and aged BMSCs with Raw 264.7 cells and found that both had the ability to promote M2 polarization (18). This could be attributed to the fact that the aged BMSCs used by Yin et al. were extracted from mice aged 6 months, which actually does not represent an aged state but rather a middle-aged state. Therefore, in this study, we utilized BMSCs from 20-month-old mice as aged BMSCs for our investigation. We initially observed that the conditioned media from aged BMSCs could upregulate the expression of inflammatory cytokines such as IL-1β, IL-6, and TNF-α in BMDMs. Next, we found

that USP7 could downregulate the innate immune response pathway and NLRP3 inflammasome pathway in senescent BMDMs. Similar to our findings, Palazon et al. discovered that USP7 and USP47 directly regulated the deubiquitination of NLRP3 protein and mainly maintained the NLRP3 pathway by preserving ASC speck formation (19). Therefore, the inflammatory pathway mediated by USP7 could serve as a drug target for ameliorating inflammatory microenvironment of bone aging.

After validating the regulatory effect of USP7 on BMDMs' inflammaging, we further investigated the impact of USP7 on BMSCs-BMDMs crosstalk. USP7-depleted senescent BMDMs alleviated their inflammaging, while also promoting the osteogenic ability of aged BMSCs co-cultured with them, mitigating the aging level of aged BMSCs. In previous studies, it was found that IL-6 and TNF-α secreted by M1 macrophages significantly inhibited the functions of BMSCs and osteoblasts (20, 21). Li and colleagues discovered that in the bone marrow of aged mice, 80% of macrophages exhibit the M1 phenotype (whereas in young mice, M1 macrophages only make up 5%), and GCA secreted by these M1 macrophages significantly inhibited osteogenic differentiation (22). Therefore, inhibiting bone inflammatory microenvironment is a crucial therapeutic approach to maintaining stem cell osteogenic differentiation and reducing bone loss.

However, following the concurrent treatment of BMDMs and BMSCs with the USP7 inhibitor P5091, young BMSCs co-cultured with BMDMs exhibited suppressed osteogenesis. Inspired by these findings, we observed that USP7 depletion, while increasing the mRNA expression of *Alp*, *Runx2*, and *Col1a1* in young BMSCs, led to

a reduction in the protein levels of ALP and COL1A1. This suggested that USP7 might be involved in post-transcriptional regulation mechanisms for ALP and COL1A1 proteins. Similarly, Kim et al. demonstrated that after USP7 depletion, the ubiquitination levels of NANOG and SOX2 increased, subsequently inhibiting self-renewal capacity and multipotency of BMSCs (23). However, through mRNA-Seq, we discovered that USP7 depletion promoted apoptosis and osteoblast differentiation in aged BMSCs, while SASP pathway was inhibited. Further, we found that USP7 depletion and P5091 could selectively induce apoptosis in aged BMSCs while promoting osteogenic differentiation and suppressing the SASP. Therefore, we validated P5091, as a potential senolytic drug, that might also affect aged BMSCs and promoted osteogenic capabilities. Farr et al. utilized dasatinib and quercetin, a classic senolytic therapy, to eliminate senescent cells in aged mice and alleviate of osteoporosis (24). However, currently there are no studies on applying the senolytic effects of P5091 to age-related osteoporosis and bone healing. It is worth noting that Lin et al. found in ovariectomy (OVX)-induced osteoporosis that P5091 exerted its therapeutic effect by inhibiting osteoclast differentiation (25). On the contrary, Xie et al. found that USP7 inhibited osteoclast differentiation by stimulating STING, thereby reducing the level of bone loss in the skull (26). The differences observed in the aforementioned studies may stem from the choice of cell and animal models. Lin et al. primarily employed peripheral blood monocytes and OVX-induced osteoporosis models, whereas Xie et al. predominantly utilized BMDMs and RANKL-induced skull bone resorption models. This suggests that our study explores the role of USP7

inhibition from the perspective of immunomodulation and cellular interactions, incorporating multiple models such as bone homeostasis and bone healing.

Through analysis of single-cell sequencing data from human femoral heads, we discovered that macrophages in the bone marrow exhibit high expression of the efferocytosis-related gene, *Mertk*. This suggests that BMDMs may play an active role in efferocytotic processes within the bone microenvironment. Therefore, through mRNA-seq analysis, we found that USP7 depletion upregulated the efferocytosis pathway in BMDMs, i.e., their ability to engulf apoptotic cells. Efferocytosis consists of three stages: the smell phase, the eating phase, and the digestion phase (27). After completing efferocytosis, macrophages undergo M2 polarization and produce anti-inflammatory cytokines (28). Indeed, this is crucial for wound healing and tissue homeostasis. In the early inflammation stages of wound healing, M1 macrophages promote initial wound healing by producing pro-inflammatory cytokines and phagocytosing apoptotic neutrophils or other apoptotic cells via efferocytosis (29). During this process, efferocytosis plays a critical role in transitioning M1 macrophages into the M2 phenotype, which contributes to tissue remodeling in the later stages of wound healing (27). However, in aging individuals, macrophages may experience impaired phagocytic and efferocytosis functions because of impaired MerTK function (30). This can lead to ineffective clearance of apoptotic cells in the aging bone microenvironment, and macrophages may be difficult to turn into M2 phenotype through efferocytosis. In this study, we observed that USP7 depletion improved the impaired efferocytosis function of senescent BMDMs, and promoted the

expression of LRP1 in senescent BMDMs. LRP1 is a key receptor involved in mediating efferocytosis (31). In atherosclerosis, LRP1 in monocytes is degraded through EPSIN1-mediated mechanisms, leading to a reduction in efferocytosis (32). Therefore, we used an LRP1 inhibitor RAP and found that LRP1 inhibition could counteract the promoting effect of USP7 on efferocytosis. Subsequently, we investigated how USP7 regulates LRP1 and found that USP7 inhibition could increase the ubiquitination of EPSIN1, thus protecting LRP1 from degradation, and consequently enhancing the efferocytosis capacity of senescent BMDMs.

Previous studies *in vitro* revealed that USP7 inhibition not only selectively eliminates aged BMSCs, promoting osteogenic differentiation, but also enhances immunomodulatory effects by improving the efferocytosis capacity of senescent BMDMs. Indeed, studies have found that the efficacy of locally applied senolytic drugs may not fully match that of systemically administered senolytic drugs (33). Moreover, the accumulation of excessive apoptotic cells can also be detrimental to tissues. Therefore, combining senolysis with efferocytosis to achieve selective apoptosis of senescent cells and their rapid clearance may represent an important research direction in anti-aging therapies (34). In bone tissue, current research has found that MFG-E8 facilitates macrophage efferocytosis and M2 polarization, thereby promoting tendon-bone healing (35). However, there is still a lack of research on efferocytosis in age-related osteoporosis and osseointegration

Consequently, this study not only explored the role of USP7 inhibition-mediated efferocytosis in osteoporosis but also further investigated its impact on

osseointegration. We *in vivo* validated the impact of USP7 inhibitor P5091 on age-related osteoporosis and osteoporotic osseointegration of mice. First, regarding osteoporosis, we observed an increased number of apoptotic cells and macrophage engulfing apoptotic cells in aged mice following systemic administration of P5091. This suggests that systemic P5091 can alleviate osteoporosis in aged mice through senolysis and efferocytosis. However, when we used RAP, we found a significant reduction in efferocytosis levels and bone mass. It indicates that promoting efferocytosis plays a crucial role in maintaining bone homeostasis and alleviating bone aging. In periodontitis, promoting macrophage efferocytosis mediated by DEL-1 has been shown to alleviate periodontal inflammation and reduce alveolar bone resorption (36). In addition to maintaining tissue homeostasis, promoting efferocytosis also contributes to tissue repair in various pathological conditions. In diabetic wounds, targeting dendritic cells with SLC7A11 helps reduce the burden of senescent cells, promoting wound healing (27). Similarly, this study found that USP7 inhibition promoted senolysis and macrophage efferocytosis during the early stage of osseointegration, i.e., 2 weeks post-implantation, while RAP inhibited this effect. However, significant osteogenesis and osseointegration effects were only observed at 4 weeks post-implantation. This may be due to the fact that, compared to young mice, in aged mice, bone resorption and stem cell migration processes are not yet completed at 2 weeks, and osteogenic activity is not sufficiently active (37). Interestingly, at 2 weeks post-implantation, there was no significant difference in osteoclastic activity around the implants between young and aged mice. However, at 4 weeks

post-implantation, the number of osteoclasts around the implants in young mice had significantly decreased, while aged mice maintained higher levels of osteoclastic activity. USP7 inhibition significantly suppressed the number of osteoclasts. This may be because USP7 inhibition promotes timely polarization of macrophages towards the M2 phenotype, thereby avoiding prolonged inflammation, which in turn prevents the maintenance of osteoclastic activity. However, unlike the femur, there are certain foreign bodies present around the implants, such as Ti particles and bacteria. USP7-mediated efferocytosis may also have an impact on the engulfment of these substances by macrophages (38). Therefore, future research could further investigate the relationship between USP7-mediated macrophage efferocytosis and the engulfment of foreign bodies such as Ti particles and bacteria around the implants.

However, this study still has several limitations. In *in vivo* experiments, there may be other immune cells, such as dendritic cells, participating in efferocytosis, but this study only explored macrophages. As for *in vitro*, further researches should delve into the molecular mechanisms underlying USP7's regulation of senolysis in aged BMSCs. Additionally, due to the limitations of the direct co-culture model for WB and qPCR detection, some experiments used an indirect co-culture model with transwells, which has certain limitations in studying efferocytosis as macrophages can only interact with BMSCs through paracrine processes.

References

1. Lane NE. Epidemiology, etiology, and diagnosis of osteoporosis. Am J Obstet Gynecol. 2006;194(2 Suppl):S3-11.

2. Brocard D, Barthet P, Baysse E, Duffort JF, Eller P, Justumus P, et al. A multicenter report on 1,022 consecutively placed ITI implants: a 7-year longitudinal study. Int J Oral Maxillofac Implants. 2000;15(5):691-700.

3. Bertl K, Ebner M, Knibbe M, Pandis N, Kuchler U, Ulm C, et al. How old is old for implant therapy in terms of early implant losses? J Clin Periodontol. 2019;46(12):1282-93.

4. Chappuis V, Avila-Ortiz G, Araújo MG, Monje A. Medication-related dental implant failure: Systematic review and meta-analysis. Clin Oral Implants Res. 2018;29 Suppl 16:55-68.

5. Bellavia D, Costa V, De Luca A, Maglio M, Pagani S, Fini M, et al. Vitamin D Level Between Calcium-Phosphorus Homeostasis and Immune System: New Perspective in Osteoporosis. Curr Osteoporos Rep. 2016.

6. Saxena Y, Routh S, Mukhopadhaya A. Immunoporosis: Role of Innate Immune Cells in Osteoporosis. Front Immunol. 2021;12:687037.

7. Ferrucci L, Fabbri E. Inflammageing: chronic inflammation in ageing, cardiovascular disease, and frailty. Nat Rev Cardiol. 2018;15(9):505-22.

8. Franceschi C, Bonafè M, Valensin S, Olivieri F, De Luca M, Ottaviani E, et al. Inflamm-aging. An evolutionary perspective on immunosenescence. Ann N Y Acad Sci. 2000;908:244-54.

9. Ma Y, Wang S, Wang H, Chen X, Shuai Y, Wang H, et al. Mesenchymal stem cells and dental implant osseointegration during aging: from mechanisms to therapy. Stem cell research & therapy. 2023;14(1):382.

10. Park J, Cho J, Song EJ. Ubiquitin-proteasome system (UPS) as a target for anticancer treatment. Arch Pharm Res. 2020;43(11):1144-61.

11. Komander D, Clague MJ, Urbé S. Breaking the chains: structure and function of the deubiquitinases. Nat Rev Mol Cell Biol. 2009;10(8):550-63.

12. He Y, Li W, Lv D, Zhang X, Zhang X, Ortiz YT, et al. Inhibition of USP7 activity selectively eliminates senescent cells in part via restoration of p53 activity. Aging cell. 2020;19(3):e13117.

13. Schmitt R. Senotherapy: growing old and staying young? Pflugers Archiv : European journal of physiology. 2017;469(9):1051-9.

14. Bartelt A, Behler-Janbeck F, Beil FT, Koehne T, Müller B, Schmidt T, et al. Lrp1 in osteoblasts controls osteoclast activity and protects against osteoporosis by limiting PDGF-RANKL signaling. Bone Res. 2018;6:4.

15. Farr JN, Khosla S. Cellular senescence in bone. Bone. 2019;121:121-33.

16. Koyuncu S, Loureiro R, Lee HJ, Wagle P, Krueger M, Vilchez D. Rewiring of the ubiquitinated proteome determines ageing in C. elegans. Nature. 2021;596(7871):285-90.

17. Ambrosi TH, Marecic O, McArdle A, Sinha R, Gulati GS, Tong X, et al. Aged skeletal stem cells generate an inflammatory degenerative niche. Nature. 2021;597(7875):256-62.

18. Yin Y, Wu R-X, He X-T, Xu X-Y, Wang J, Chen F-M. Influences of age-related changes in mesenchymal stem cells on macrophages during in-vitro culture. Stem cell research & therapy. 2017;8(1):153.

19. Palazón-Riquelme P, Worboys JD, Green J, Valera A, Martín-Sánchez F, Pellegrini C, et al. USP7 and USP47 deubiquitinases regulate NLRP3 inflammasome activation. EMBO reports. 2018;19(10).

20. Harmer D, Falank C, Reagan MR. Interleukin-6 Interweaves the Bone Marrow Microenvironment, Bone Loss, and Multiple Myeloma. Front Endocrinol (Lausanne). 2018;9:788.

21. Sun W, Meednu N, Rosenberg A, Rangel-Moreno J, Wang V, Glanzman J, et al. B cells inhibit bone formation in rheumatoid arthritis by suppressing osteoblast differentiation. Nature communications. 2018;9(1):5127.

22. Li C-J, Xiao Y, Sun Y-C, He W-Z, Liu L, Huang M, et al. Senescent immune cells release grancalcin to promote skeletal aging. Cell metabolism. 2021;33(10).

23. Kim YJ, Park KH, Lee K-M, Chun Y-M, Lee JW. Deubiquitinating Enzyme USP7 Is Required for Self-Renewal and Multipotency of Human Bone Marrow-Derived Mesenchymal Stromal Cells. International journal of molecular sciences. 2022;23(15).

24. Farr JN, Xu M, Weivoda MM, Monroe DG, Fraser DG, Onken JL, et al. Targeting cellular senescence prevents age-related bone loss in mice. Nat Med. 2017;23(9):1072-9.

25. Lin Y-C, Zheng G, Liu H-T, Wang P, Yuan W-Q, Zhang Y-H, et al. USP7 promotes the osteoclast differentiation of CD14+ human peripheral blood monocytes in osteoporosis via HMGB1 deubiquitination. J Orthop Translat. 2023;40:80-91.

26. Xie Z, Wu Y, Shen Y, Guo J, Yuan P, Ma Q, et al. USP7 Inhibits Osteoclastogenesis via Dual Effects of Attenuating TRAF6/TAK1 Axis and Stimulating STING Signaling. Aging Dis. 2023;14(6):2267-83.

27. Maschalidi S, Mehrotra P, Keçeli BN, De Cleene HKL, Lecomte K, Van der Cruyssen R, et al. Targeting SLC7A11 improves efferocytosis by dendritic cells and wound healing in diabetes. Nature. 2022;606(7915):776-84.

28. Boada-Romero E, Martinez J, Heckmann BL, Green DR. The clearance of dead cells by efferocytosis. Nat Rev Mol Cell Biol. 2020;21(7):398-414.

29. Kim H, Wang SY, Kwak G, Yang Y, Kwon IC, Kim SH. Exosome-Guided Phenotypic Switch of M1 to M2 Macrophages for Cutaneous Wound Healing. Adv Sci (Weinh). 2019;6(20):1900513.

30. Rymut N, Heinz J, Sadhu S, Hosseini Z, Riley CO, Marinello M, et al. Resolvin D1 promotes efferocytosis in aging by limiting senescent cell-induced MerTK cleavage. FASEB journal : official publication of the Federation of American Societies for Experimental Biology. 2020;34(1):597-609.

31. Doddapattar P, Dev R, Ghatge M, Patel RB, Jain M, Dhanesha N, et al. Myeloid Cell PKM2 Deletion Enhances Efferocytosis and Reduces Atherosclerosis. Circ Res. 2022;130(9):1289-305.

32. Brophy ML, Dong Y, Tao H, Yancey PG, Song K, Zhang K, et al. Myeloid-Specific Deletion of Epsins 1 and 2 Reduces Atherosclerosis by Preventing LRP-1 Downregulation. Circ Res. 2019;124(4).

33. Farr JN, Saul D, Doolittle ML, Kaur J, Rowsey JL, Vos SJ, et al. Local senolysis in aged mice only partially replicates the benefits of systemic senolysis. The Journal of clinical investigation. 2023;133(8).

34. Mehrotra P, Ravichandran KS. Drugging the efferocytosis process: concepts and opportunities. Nat Rev Drug Discov. 2022;21(8):601-20.

35. Geng R, Lin Y, Ji M, Chang Q, Li Z, Xu L, et al. MFG-E8 promotes tendon-bone healing by regualting macrophage efferocytosis and M2 polarization after anterior cruciate ligament reconstruction. J Orthop Translat. 2022;34:11-21.

36. Kourtzelis I, Li X, Mitroulis I, Grosser D, Kajikawa T, Wang B, et al. DEL-1 promotes macrophage efferocytosis and clearance of inflammation. Nat Immunol. 2019;20(1):40-9.

37. Liu R, Gao Y, Huang L, Shi B, Yin X, Zou S. Alpha-ketoglutarate up-regulates autophagic activity in peri-implant environment and enhances dental implant osseointegration in osteoporotic mice. J Clin Periodontol. 2023;50(5):671-83.

38. Wang X, Li Y, Feng Y, Cheng H, Li D. Macrophage polarization in aseptic bone resorption around dental implants induced by Ti particles in a murine model. J Periodontal Res. 2019;54(4):329-38.

Acknowledgement: We acknowledge the funding from the National Natural Science Foundation of China (81970966, 82001084), Natural Science Foundation of Sichuan Province (2023NSFSC1513, 2023NSFSC0574).

Figures

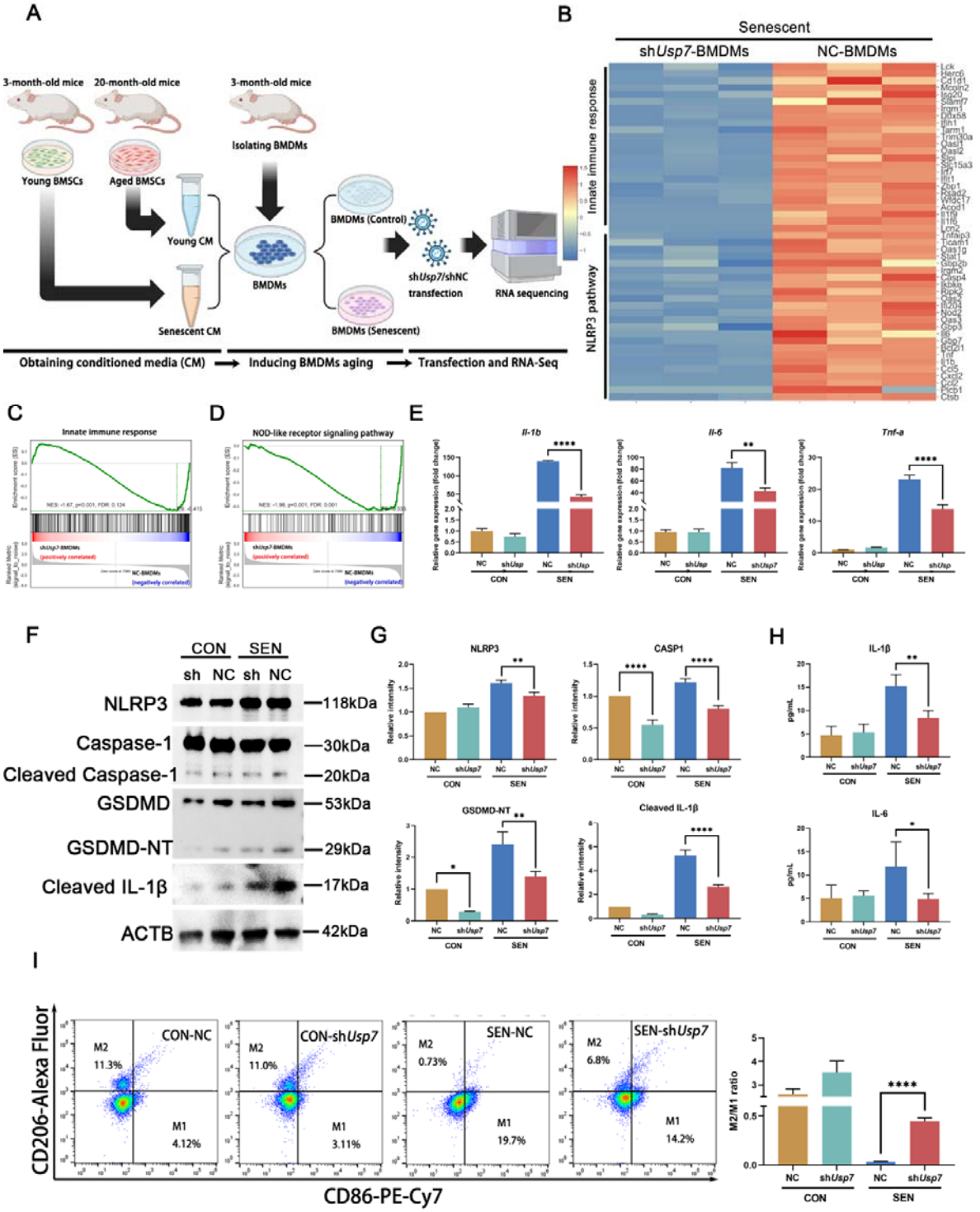
A
3-month-old mice
20-month-old mice
3-month-old mice
Isolating BMDMs
Young BMSCs
Aged BMSCs
Young CM
Senescent CM
BMDMs
BMDMs (Control)
shUsp7/shNC transfection
BMDMs (Senescent)
RNA sequencing
Obtaining conditioned media (CM)
Inducing BMDMs aging
Transfection and RNA-Seq
B
Senescent
shUsp7-BMDMs
NC-BMDMs
Innate immune response
NLRP3 pathway
C
Innate immune response
D
NOD-like receptor signaling pathway
E
Il-1b
Il-6
Tnf-a
CON
SEN
F
CON
SEN
sh
NC
NLRP3
Caspase-1
Cleaved Caspase-1
GSDMD
GSDMD-NT
Cleaved IL-1β
ACTB
118kDa
30kDa
20kDa
53kDa
29kDa
17kDa
42kDa
G
NLRP3
CASP1
GSDMD-NT
Cleaved IL-1β
H
IL-1β
IL-6
I
CD206-Alexa Fluor
CD86-PE-Cy7
CON-NC
CON-shUsp7
SEN-NC
SEN-shUsp7
M2
11.3%
M1
4.12%
M2
11.0%
M1
3.11%
M2
0.73%
M1
19.7%
M2
6.8%
M1
14.2%
M2/M1 ratio

Fig. 1. **USP7 depletion inhibited inflammaging in senescent BMDMs via NLRP3 pathway.** (**A**) Illustration of the experimental workflow for acquiring senescent BMDMs, USP7 depletion, and mRNA-Seq. (**B**) Heatmap of representative core genes associated with innate immune response and NLRP3 inflammasome pathway. (**C-D**) GSEA showed downregulated innate immune response and NLRP3 inflammasome pathway in USP7-depleted senescent BMDMs. **(E)** qPCR results of maker genes of inflammaging in normal/senescent BMDMs transfected with sh*Usp7* or NC for 4 d, *n*=3. (**F**) Western blot and (**G**) quantification of NLRP3, Caspase-1, GSDMD, IL-1β and β-actin in different group of BMDMs transfected with sh*Usp7* or NC for 4 d, *n*=3. (**H**) ELISA showed the production of IL-1β and IL-6 in supernatant of normal/senescent BMDMs transfected with sh*Usp7* or NC for 4 d, *n*=3. (**I**) Flow cytometry analysis for M2/M1 polarization of normal/senescent BMDMs transfected with sh*Usp7* or NC for 4 d, *n*=3. CON, control BMDMs; SEN, senescent BMDMs; NC, BMDMs transfected with NC lentivirus; sh*Usp7*, BMDMs transfected with sh*Usp7* lentivirus. Data are presented as means ± SD. $^{*}P < 0.05$, $^{**}P < 0.01$, $^{***}P < 0.001$, $^{****}P < 0.0001$.

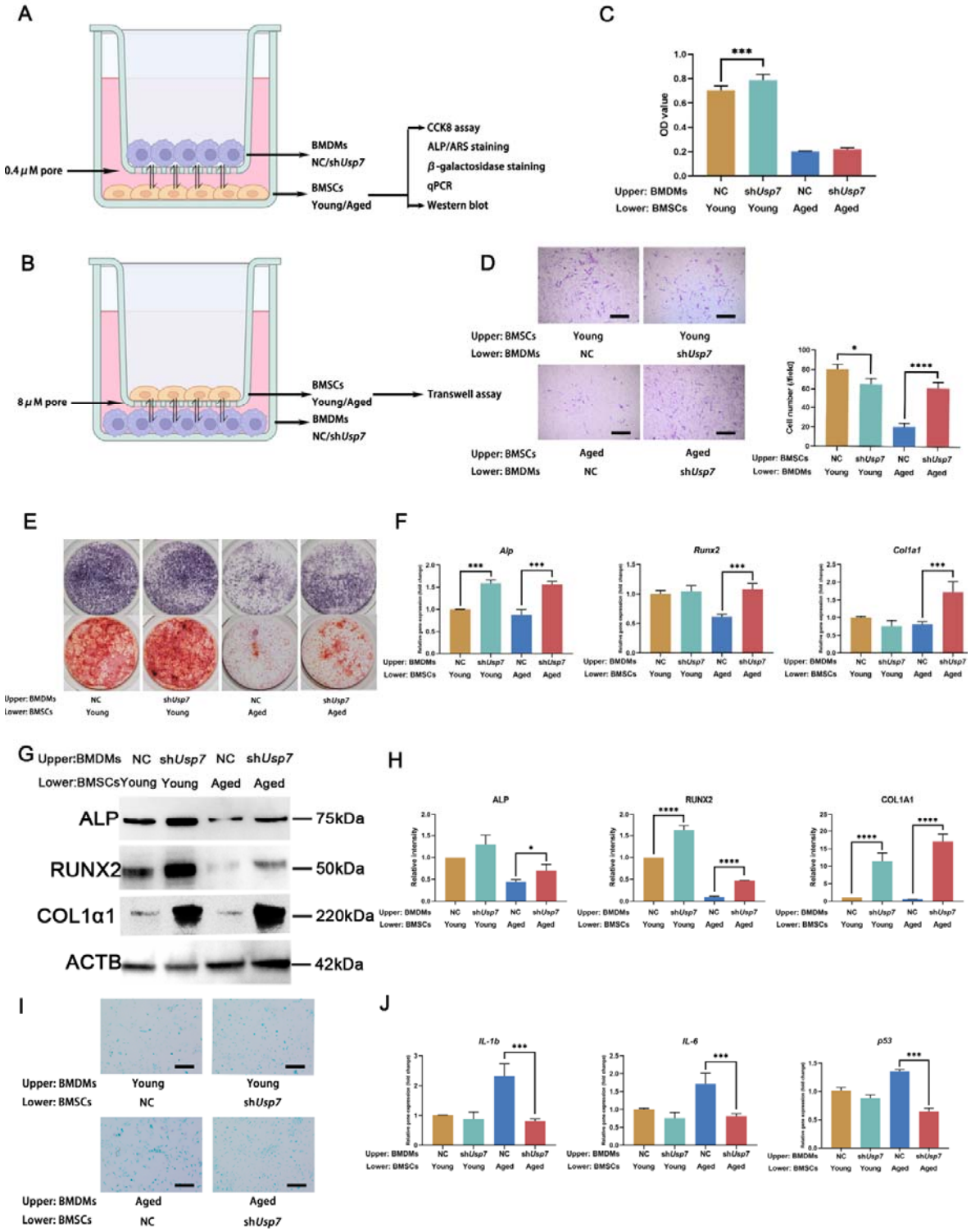
A
0.4 μM pore
BMDMs
NC/shUsp7
BMSCs
Young/Aged
CCK8 assay
ALP/ARS staining
β-galactosidase staining
qPCR
Western blot
B
8 μM pore
BMSCs
Young/Aged
BMDMs
NC/shUsp7
Transwell assay
C
OD value
Upper: BMDMs NC shUsp7 NC shUsp7
Lower: BMSCs Young Young Aged Aged
D
Upper: BMSCs Young Young
Lower: BMDMs NC shUsp7
Upper: BMSCs Aged Aged
Lower: BMDMs NC shUsp7
Cell number (field)
Upper: BMSCs NC shUsp7 NC shUsp7
Lower: BMDMs Young Young Aged Aged
E
Upper: BMDMs NC shUsp7 NC shUsp7
Lower: BMSCs Young Young Aged Aged
F
Alp
Runx2
Col1a1
Upper: BMDMs NC shUsp7 NC shUsp7
Lower: BMSCs Young Young Aged Aged
G
Upper:BMDMs NC shUsp7 NC shUsp7
Lower:BMSCs Young Young Aged Aged
ALP
RUNX2
COL1α1
ACTB
75kDa
50kDa
220kDa
42kDa
H
ALP
RUNX2
COL1A1
Relative intensity
Upper: BMDMs NC shUsp7 NC shUsp7
Lower: BMSCs Young Young Aged Aged
I
Upper: BMDMs Young Young
Lower: BMSCs NC shUsp7
Upper: BMDMs Aged Aged
Lower: BMSCs NC shUsp7
J
IL-1b
IL-6
p53
Upper: BMDMs NC shUsp7 NC shUsp7
Lower: BMSCs Young Young Aged Aged

Fig. 2. USP7-depleted BMDMs enhanced osteogenesis of aged BMSCs. (**A-B**) Illustration of the indirect co-culture model of BMSCs and BMDMs. (**C**) CCK8 assay for determining cell viability of young/aged BMSCs co-cultured with different BMDMs for 72 h, *n*=6. (**D**) Representative images and quantitative analysis of migration capacity of aged/young BMSCs co-cultured with different BMDMs for 24 h, *n*=3, scale bar, 50μM. (**E**) Representative images of ALP and ARS staining in different groups of BMSCs after initiating osteogenic induction for 7 and 14 d. (**F**) qPCR results of osteogenic markers in different groups of BMSCs after initiating osteogenic induction for 7 d, *n*=3. (**G**) Western blot and (**H**) quantification of ALP, RUNX2, COL1α1, and β-actin in different group of BMSCs after initiating osteogenic induction for 7 d, *n*=3. (**I**) Representative images of β-galactosidase staining of different BMSCs, scale bar, 50μM. (**J**) qPCR results of SASP markers in different groups of BMSCs, *n*=3. NC, BMDMs transfected with NC lentivirus; sh*Usp7*, BMDMs transfected with sh*Usp7* lentivirus. Data are presented as means ± SD. $^{*}P < 0.05$, $^{**}P < 0.01$, $^{***}P < 0.001$, $^{****}P < 0.0001$.

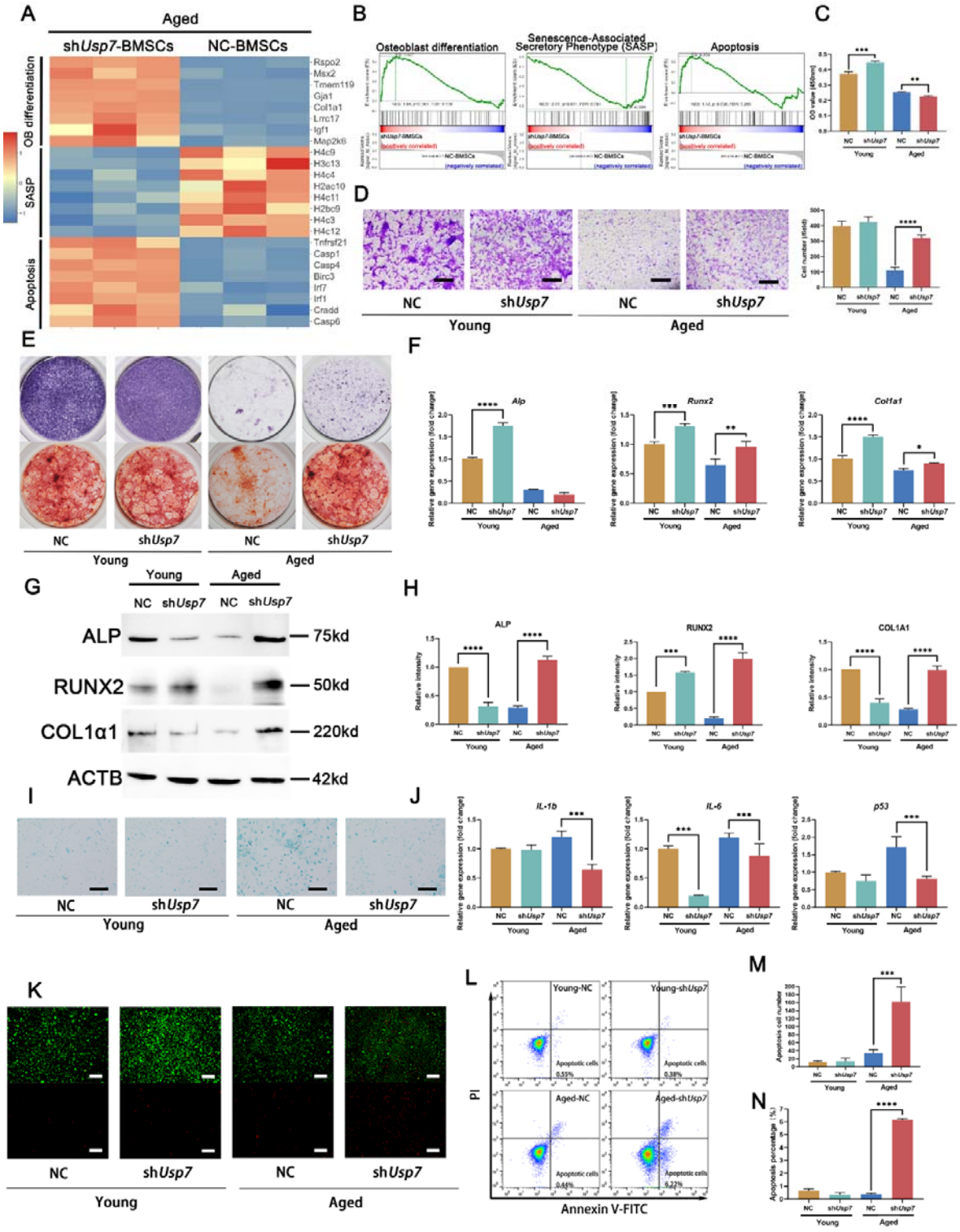

Fig. 3. USP7 depletion promoted osteogenesis of aged BMSCs via senolysis. (**A**)

Heatmap of representative core genes associated with osteoblast differentiation,

SASP, and apoptosis pathway. (**B**) GSEA showed upregulated osteoblast differentiation, downregulated SASP and apoptosis pathway in USP7-depleted aged BMSCs. (**C**) CCK8 assay for determining cell viability of young/aged BMSCs transfected with NC or sh*Usp7* lentivirus for 72 h, *n*=6. (**D**) Representative images and quantitative analysis of migration capacity of aged/young BMSCs for 24 h, *n*=3, scale bar, 50μM. (**E**) Representative images of ALP and ARS staining in different groups of BMSCs after initiating osteogenic induction for 7 and 14 d. (**F**) qPCR results of osteogenic markers in different groups of BMSCs after initiating osteogenic induction for 7 d, *n*=3. (**G**) Western blot and (**H**) quantification of ALP, RUNX2, COL1α1, and β-actin in different group of BMSCs after initiating osteogenic induction for 7 d, *n*=3. (**I**) Representative images of SA-β-gal staining of different BMSCs, scale bar, 50μM. (**J**) qPCR results of SASP markers in different groups of BMSCs, *n*=3. (**K**) Representative images of live/dead staining of BMSCs after transfected with NC or sh*Usp7* lentivirus for 72 h, green color indicates live cells, red color indicates dead cells, scale bar, 150μM. (**L**) Flow cytometry for apoptosis in BMSCs after transfected with NC or sh*Usp7* lentivirus for 72 h. (**M-N**) Quantification of live/dead staining and flow cytometry to evaluate apoptosis level in BMSCs, *n*=3. NC, BMSCs transfected with NC lentivirus; sh*Usp7*, BMSCs transfected with sh*Usp7* lentivirus. Data are presented as means ± SD. $^{*}P < 0.05$, $^{**}P < 0.01$, $^{***}P < 0.001$, $^{****}P < 0.0001$.

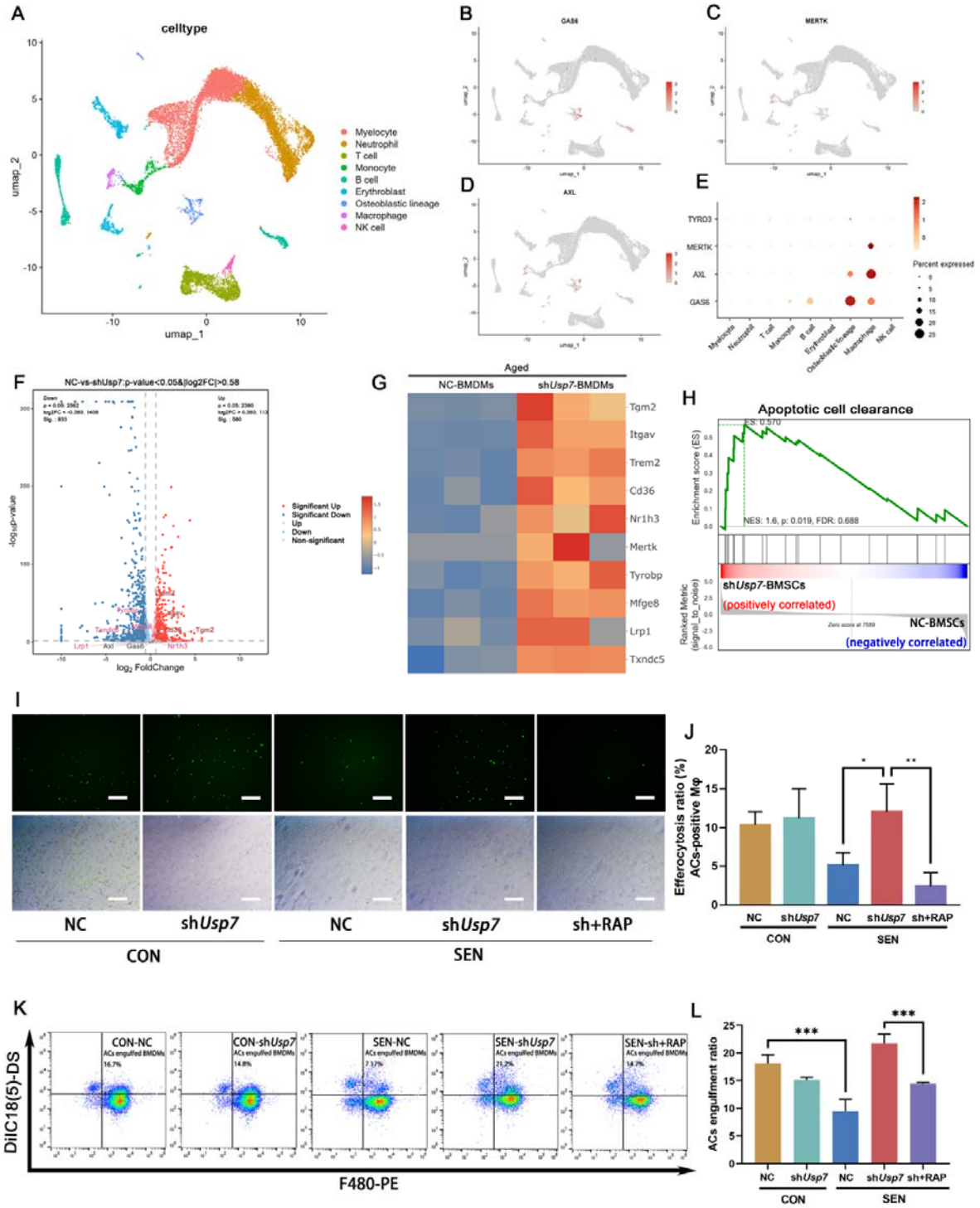

Fig. 4. **USP7 depletion promoted efferocytosis in senescent BMDMs partially through LRP1** (**A**) UMAP plot analysis of the human femoral head bone

marrow datasets of scRNAseq based on GSE169396. **(B-D)** UMAP plots of the expression of Gas6, Axl, and Mertk. **(E)** Dot plot of efferocytosis marker gene expression in myelocyte, neutrophil, T cell, monocyte, erythroblast, osteoblastic lineage, macrophage, and NK cell. **(F)** Volcano plot of USP7-depleted and NC senescent BMDMs of differentially expressed genes, and efferocytosis-related genes were marked. **(G)** Heatmap of representative core genes associated with apoptotic cell clearance. (**H**) GSEA showed upregulated apoptotic clearance pathway in USP7-depleted senescent BMDMs. (**I-J**) Representative images and quantitative analysis of efferocytosis ratio of control/senescent BMDMs co-cultured with apoptotic Jurkat cells for 24 h, n=3, scale bar, 150μM. (**K-L**) Flow cytometry analysis for evaluating efferocytosis capacity of control/senescent BMDMs co-cultured with apoptotic Jurkat cells for 24 h, n=3. CON, control BMDMs; SEN, senescent BMDMs; NC, BMDMs transfected with NC lentivirus; sh*Usp7*, BMDMs transfected with sh*Usp7* lentivirus. RAP, receptor-associated-protein. Data are presented as means ± SD. *P < 0.05, **P < 0.01, ***P < 0.001, ****P < 0.0001.

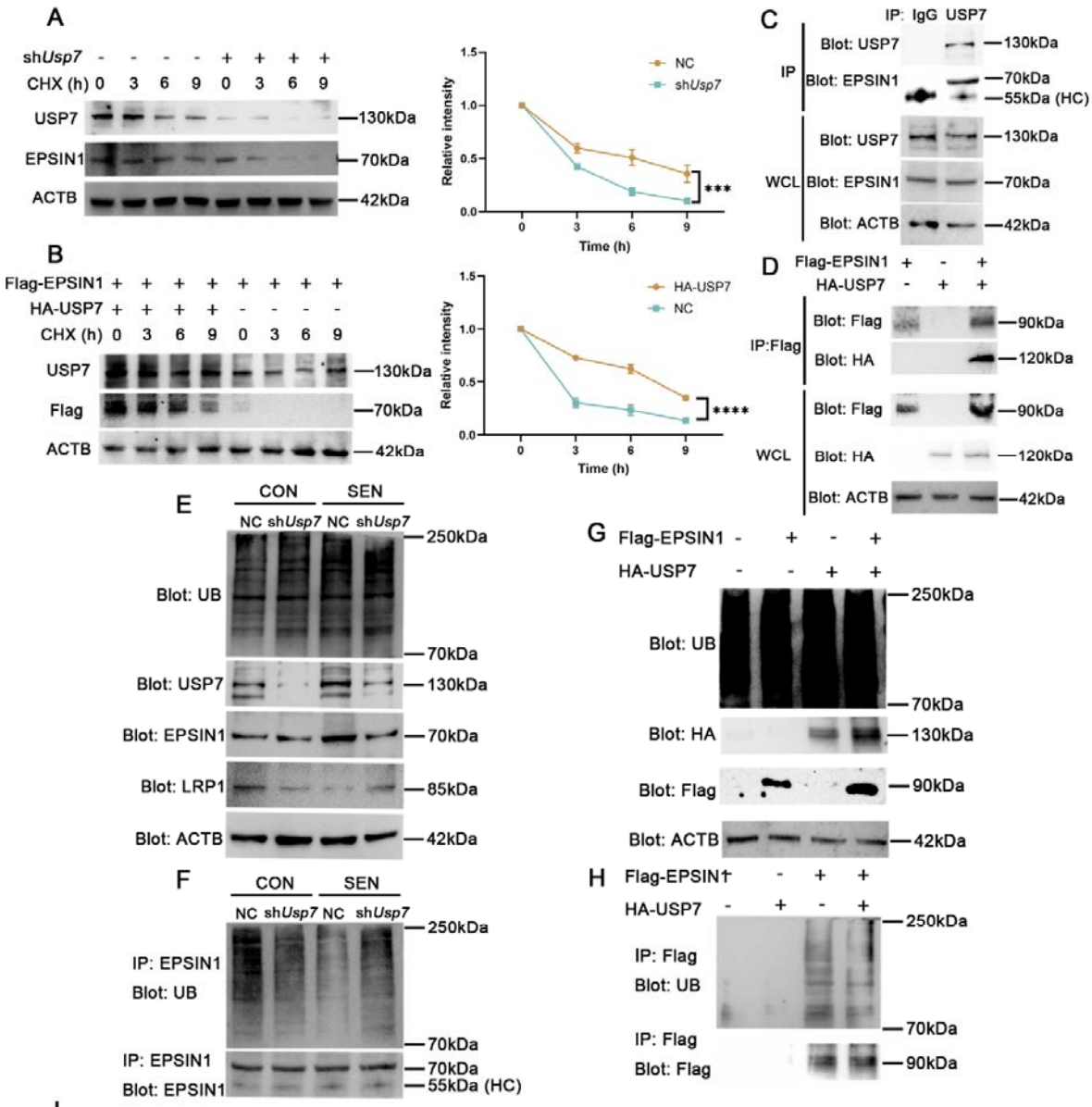
A
shUsp7 - - - - + + + +
CHX (h) 0 3 6 9 0 3 6 9
USP7
EPSIN1
ACTB
130kDa
70kDa
42kDa
NC
shUsp7
Relative intensity
Time (h)
***
B
Flag-EPSIN1 + + + + + + + +
HA-USP7 + + + + - - - -
CHX (h) 0 3 6 9 0 3 6 9
USP7
Flag
ACTB
130kDa
70kDa
42kDa
HA-USP7
NC
****
C
IP: IgG USP7
IP
Blot: USP7
Blot: EPSIN1
130kDa
70kDa
55kDa (HC)
WCL
Blot: ACTB
42kDa
D
Flag-EPSIN1 + - +
HA-USP7 - + +
IP:Flag
Blot: Flag
Blot: HA
90kDa
120kDa
E
CON SEN
NC shUsp7 NC shUsp7
Blot: UB
Blot: USP7
Blot: EPSIN1
Blot: LRP1
Blot: ACTB
250kDa
70kDa
130kDa
85kDa
42kDa
F
IP: EPSIN1
Blot: UB
Blot: EPSIN1
55kDa (HC)
G
Flag-EPSIN1 - + - +
HA-USP7 - - + +
Blot: HA
Blot: Flag
H
Flag-EPSIN1 - + +
HA-USP7 - + - +
IP: Flag
I
Senescent BMDMs (NC)
LRP1
EPSIN1
Reduced protein level of LRP1
Efferocytosis
Senescent BMDMs (USP7 depleted)
EPSIN1 degradation
Elevated protein level of LRP1
USP7
USP7 inhibitor/USP7 depletion

Fig. 5. **USP7 depletion mediated ubiquitin-dependent degradation of EPSIN1 to stabilize LRP1** Immunoblot of EPSIN1 in BMDMs when USP7 was overexpressed (**A**) or depleted (**B**) genetically with 20 μmol/L CHX for different times as indicated. (**C**) Interaction analysis of USP7 and EPSIN1 in BMDMs was detected using co-IP. (**D**) BMDMs was transfected with HA-USP7 and Flag-EPSIN1. Interaction of HA-USP7 and Flag-EPSIN1 was detected using co-IP. (**E**) Immunoblot analysis of ubiquitin, USP7, EPSIN1, and LRP1 in control/senescent BMDMs transfected with NC of sh*Usp7* lentivirus, followed by (**F**) co-IP with anti-EPSIN1, probed with anti-ubiquitin and anti-EPSIN1 in control/senescent BMDMs transfected with NC of sh*Usp7* lentivirus. (**G**) Immunoblot analysis of ubiquitin, HA, and Flag in BMDMs transfected with FLAG-EPSIN1, HA-USP7 and both, followed by (**H**) co-IP with anti-FLAG, probed with anti-ubiquitin and anti-Flag. (**I**) Illustration of USP7 regulating efferocytosis via EPSIN1/LRP1 pathway. CON, control BMDMs; SEN, senescent BMDMs; NC, BMDMs transfected with NC lentivirus; sh*Usp7*, BMDMs transfected with sh*Usp7* lentivirus. Data are presented as means ± SD. $^{*}P < 0.05$, $^{**}P < 0.01$, $^{***}P < 0.001$, $^{****}P < 0.0001$.

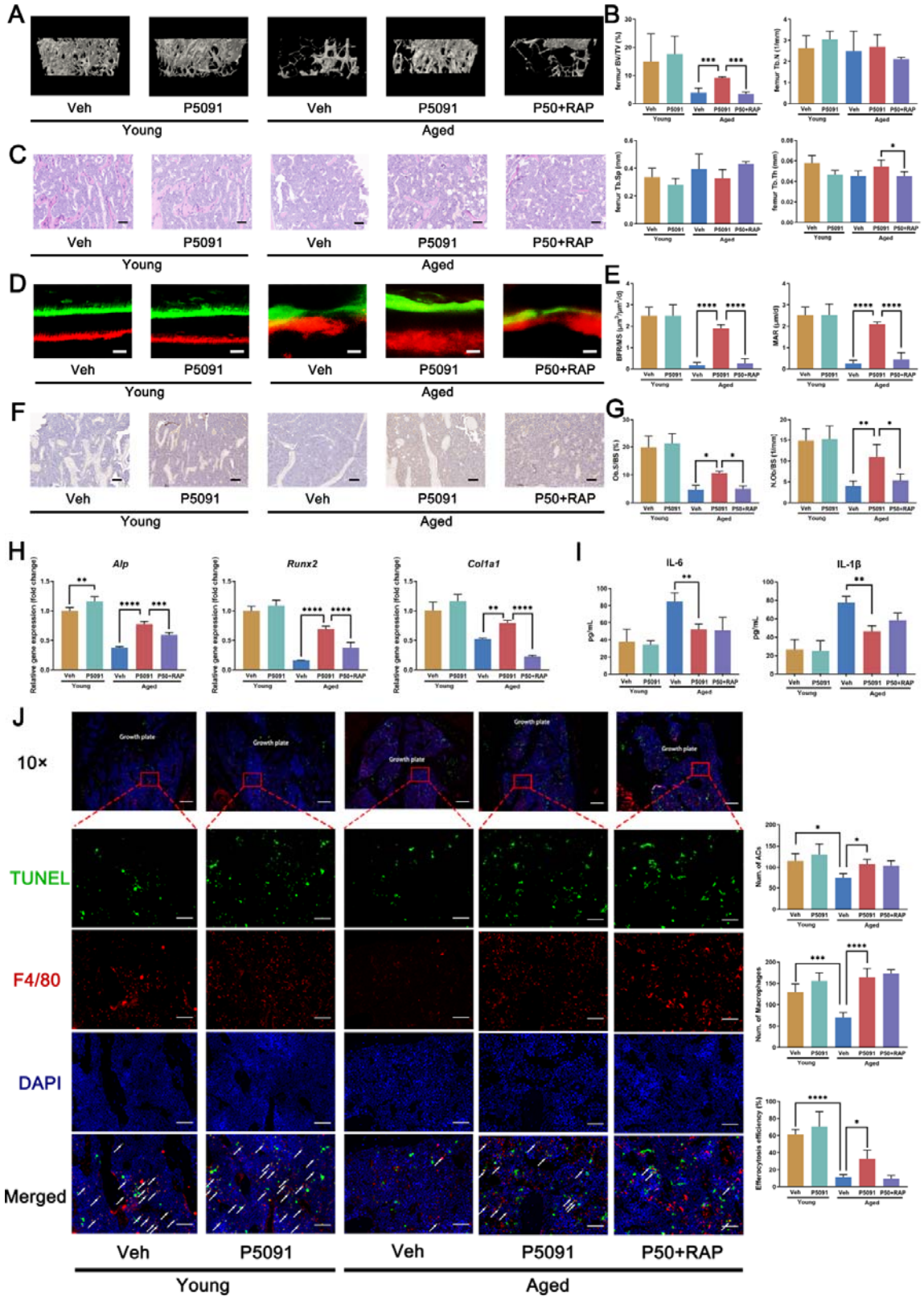
A
Veh
P5091
Veh
P5091
P50+RAP
Young
Aged
B
femur BV/TV (%)
femur Tb.N (1/mm)
femur Tb.Sp (mm)
femur Tb.Th (mm)
C
D
E
BFR/MS (μm³/μm²/d)
MAR (μm/d)
F
G
Ob.S/BS (%)
N.Ob/BS (1/mm)
H
Alp
Runx2
Col1a1
Relative gene expression (fold change)
I
IL-6
IL-1β
pg/mL
J
10×
Growth plate
TUNEL
F4/80
DAPI
Merged
Num. of ACs
Num. of Macrophages
Efferocytosis efficiency (%)

Fig. 6. **P5091 promoted osteoporosis in femurs of aged mice via efferocytosis (A**) Representative three-dimensional reconstruction images of femoral trabecular bone (**B**) Quantitative MicroCT analysis of femoral trabecular bone, *n*=5. **(C)** Representative images of H&E staining of femurs. (**D-E**) Representative images of calcein and Alizarin Red S double-label fluorescence staining of femurs followed by quantitative analysis of MAR (mineralization apposition rate) and BFR/MS (bone formation rate per bone surface), *n*=5, scale bar, 20μM. (**F-G**) Representative images of immunohistochemical staining for ALP followed by quantitative analysis of N.Ob/BS (number of osteoblast per bone surface) and Ob.S/BS (osteoblast surface per bone surface), *n*=5, scale bar, 100μM. (**H**) qPCR results of osteogenic markers in femurs from different groups of mice, *n*=5. (**I**) SASP marker, serum IL-1β and IL-6 analyzed by ELISA, *n*=5. **(J**) Representative immunofluorescence images of macrophages and apoptotic cells around the growth plate of femurs, and white arrows indicated the apoptotic cells engulfed by macrophages, followed by quantitative analysis of number of apoptotic cells, number of macrophages, and number of apoptotic cells engulfed by macrophages (efferocytosis efficiency), *n*=5, scale bar, 100μM. Veh, vehicle; RAP, receptor-associated-protein; ACs, apoptotic cells. Data are presented as means ± SD. **P* < 0.05, ***P* < 0.01, ****P* < 0.001, *****P* < 0.0001.

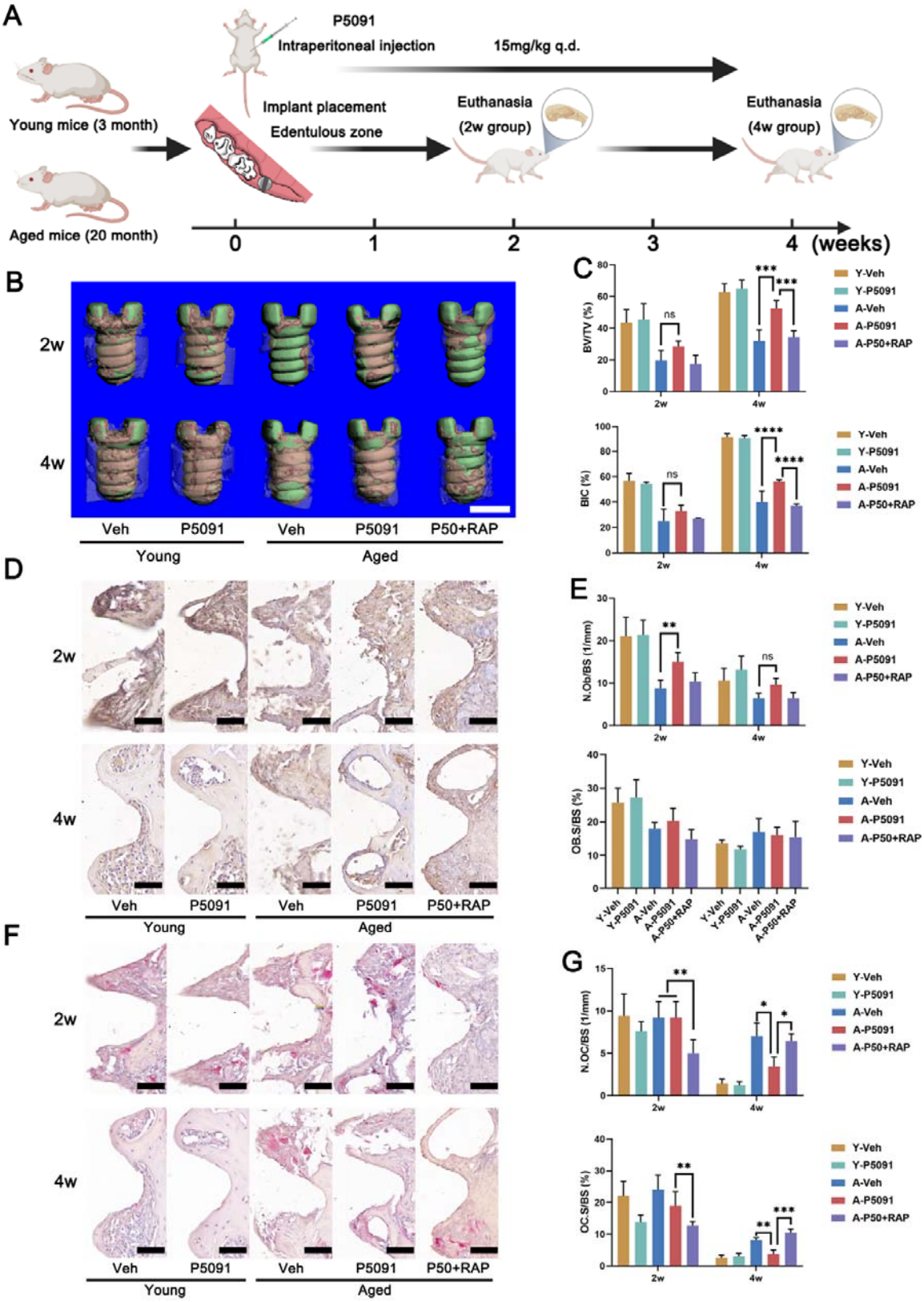
A
P5091
Intraperitoneal injection
15mg/kg q.d.
Young mice (3 month)
Implant placement
Edentulous zone
Euthanasia
(2w group)
Euthanasia
(4w group)
Aged mice (20 month)
0
1
2
3
4 (weeks)
B
2w
4w
Veh
P5091
Veh
P5091
P50+RAP
Young
Aged
C
BV/TV (%)
BIC (%)
ns
***
****
2w
4w
Y-Veh
Y-P5091
A-Veh
A-P5091
A-P50+RAP
D
2w
4w
Veh
P5091
Veh
P5091
P50+RAP
Young
Aged
E
N.Ob/BS (1/mm)
OB.S/BS (%)
**
ns
Y-Veh
Y-P5091
A-Veh
A-P5091
A-P50+RAP
F
2w
4w
Veh
P5091
Veh
P5091
P50+RAP
Young
Aged
G
N.OC/BS (1/mm)
OC.S/BS (%)
**
*
***

Fig. 7. **P5091 promoted early stage of osteoporotic osseointegration in aged mice**

(A) The schematic diagram illustrating the process of implantation in young and aged mice along with P5091 injection. **(B**) Representative three-dimensional reconstruction images of bone tissue around implant, scale bar. 600μm. (**C**) Quantitative MicroCT analysis of bone tissue around implant, *n*=5. **(D-E)** Representative images of immunohistochemical staining for ALP followed by quantitative analysis of N.Ob/BS (number of osteoblast per bone surface) and Ob.S/BS (osteoblast surface per bone surface), *n*=5, scale bar, 60μM. (**F-G**) Representative images of TRAP staining followed by quantitative analysis of N.OC/BS (number of osteoclast per bone surface) and OC.S/BS (osteoclast surface per bone surface), *n*=5, scale bar, 60μM. Veh, vehicle; RAP, receptor-associated-protein; ACs, apoptotic cells. Data are presented as means ± SD. *$P < 0.05$, **$P < 0.01$, ***$P < 0.001$, ****$P < 0.0001$.

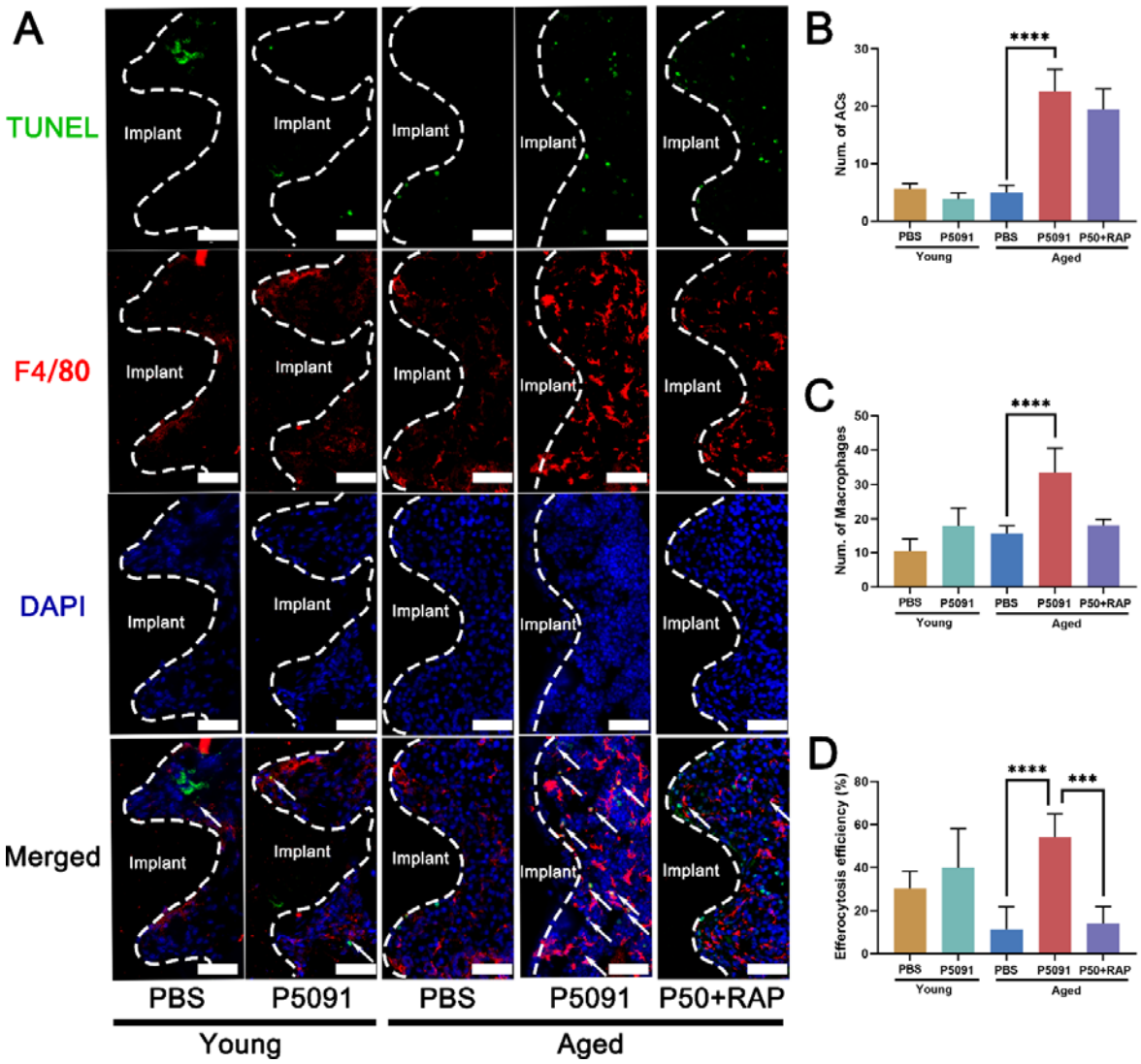

Fig. 8 P5091 promoted efferocytosis at early stage of osseointegration in aged mice (A) Representative immunofluorescence images of macrophages and apoptotic cells around the implants, and white arrows indicated the apoptotic cells engulfed by macrophages, followed by quantitative analysis of number of apoptotic cells, number of macrophages, and number of apoptotic cells engulfed by macrophages (efferocytosis efficiency), n=5. Veh, vehicle; RAP, receptor-associated-protein; ACs, apoptotic cells. Data are presented as means ± SD. *P < 0.05, **P < 0.01, ***P < 0.001, ****P < 0.0001.